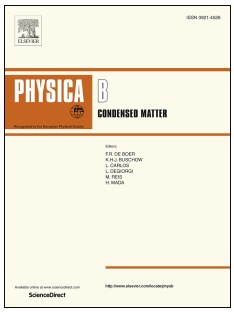
This is the accepted manuscript version of the contribution published as:

Farani, M.R., Esmaeilidehkordi, M., Alipourfard, I., **Azarian, M.**, Huh, Y.S. (2025): Utilizing armchair and zigzag nanoribbons for improved detection of SO_2 toxicity with graphene biosensor
Physica B **696** , art. 416599

The publisher's version is available at:

https://doi.org/10.1016/j.physb.2024.416599

Journal Pre-proof



Utilizing Armchair and Zigzag Nanoribbons for Improved Detection of SO_2 Toxicity with Graphene Biosensor

Marzieh Ramezani Farani, Mohammadreza Esmaeilidehkordi, Iraj Alipourfard, Maryam Azarian, Yun Suk Huh

PII: S0921-4526(24)00940-2

DOI: https://doi.org/10.1016/j.physb.2024.416599

Reference: PHYSB 416599

To appear in: *Physica B: Physics of Condensed Matter*

Received Date: 28 May 2024

Revised Date: 27 August 2024

Accepted Date: 4 October 2024

Please cite this article as: M. Ramezani Farani, M. Esmaeilidehkordi, I. Alipourfard, M. Azarian, Y.S. Huh, Utilizing Armchair and Zigzag Nanoribbons for Improved Detection of SO_2 Toxicity with Graphene Biosensor, *Physica B: Physics of Condensed Matter*, https://doi.org/10.1016/j.physb.2024.416599.

This is a PDF file of an article that has undergone enhancements after acceptance, such as the addition of a cover page and metadata, and formatting for readability, but it is not yet the definitive version of record. This version will undergo additional copyediting, typesetting and review before it is published in its final form, but we are providing this version to give early visibility of the article. Please note that, during the production process, errors may be discovered which could affect the content, and all legal disclaimers that apply to the journal pertain.

© 2024 Published by Elsevier B.V.

"Original Research"

Utilizing Armchair and Zigzag Nanoribbons for Improved Detection of SO_2 Toxicity with Graphene Biosensor

Marzieh Ramezani Farani[a, *], Mohammadreza Esmaeilidehkordi[b], Iraj Alipourfard[c], Maryam Azarian[d,e], Yun Suk Huh[a,*]

[a] *Department of Biological Sciences and Engineering, Inha University, 100 Inha-ro, Incheon, 22212, Republic of Korea. farani.marzi@gmail.com*
[b] *Department of Electrical and Computer Engineering, Isfahan University of Technology, Isfahan 8415683111, Iran. mohamadreza_esmaeili@alumni.iut.ac.ir*
[c]*Institute of Physical Chemistry, Polish Academy of Science, Warsaw, Poland. Irajbio@gmail.com*
[d]*Department of Bioanalytical Ecotoxicology,UFZ– Helmholtz Centre for Environmental Research, Leipzig, Germany.*
[e]*Department of Radiology, Charité - Universitätsmedizin Berlin, Berlin, Germany. azarian.maryam@gmail.com*

***Corresponding authors:**

Marzieh Ramezani Farani, *Department of Biological Sciences and Engineering, Inha University, 100 Inha-ro, Incheon, 22212, Republic of Korea*

Tel.: +82-10-9609-1367

Email: farani.marzi@inha.ac.kr **;** farani.marzi@gmail.com

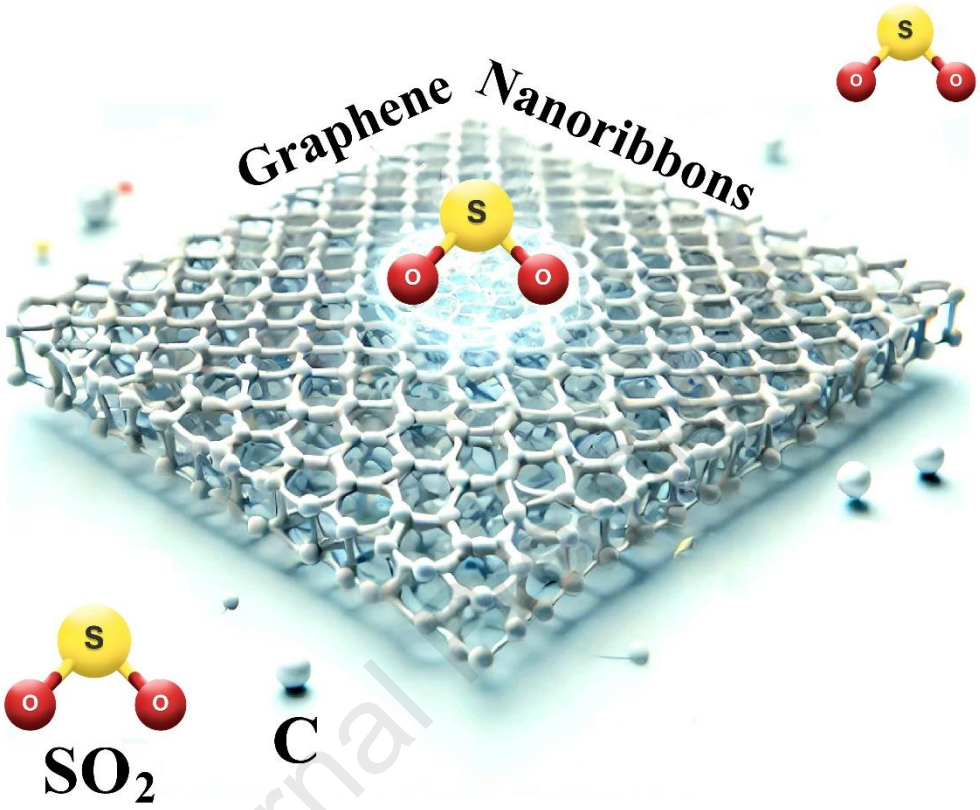
Yun Suk Huh, *Department of Biological Sciences and Engineering, Inha University, 100 Inha-ro, Incheon, 22212, Republic of Korea*

Tel.: +82-10-9633-6377

Email: yunsuk.huh@inha.ac.kr

Journal Pre-proof

Graphical Abstract



Journal Pre-proof

Journal Pre-proof

Abstract

Graphene nanoribbons (GNRs), with their distinctive structural and electronic characteristics, offer significant potential for use as biosensors in the detection of sulfur dioxide (SO_2) levels. This study employs Density Functional Theory (DFT) to evaluate the sensitivity of armchair graphene nanoribbons (AGNRs) to SO_2 gas. Specifically, we investigate the influence of SO_2 molecules on the electronic and transport characteristics of both pure and Cr-doped zigzag graphene nanoribbons (ZGNRs) and Cr-doped AGNRs. Key electronic properties, including band structure, adsorption energy, and density of states (DOS), were analyzed following SO_2 adsorption. The results indicate that Cr doping leads to significant changes in the electronic properties of AGNRs upon SO_2 exposure, including alterations in the Fermi surface that result in band separation and the formation of a forbidden band. The adsorption energy of Cr-doped AGNR increased from 0.07 eV (pristine AGNR) to 0.55 eV (Cr-doped AGNR), nearly eight times higher, indicating strong chemisorption of SO_2. These findings suggest that Cr-doped AGNRs exhibit high sensitivity to SO_2, making them promising candidates for gas detection. Furthermore, this study reveals that SO_2 adsorption in the armchair direction results in a more pronounced peak-to-valley ratio compared to the zigzag direction, highlighting distinct characteristics in SO_2 adsorption behavior. These findings could facilitate the development of advanced sensors with improved sensitivity and selectivity for environmental monitoring and safety applications.

Keywords: *Semiconductor nanostructures; Biosensors; Sulfur dioxide (SO_2) detection; ArmchairGraphene Nanoribbons (AGNR); Density functional theory (DFT); Cr-doped*

Highlights:

- 5-ZGNR and 5-AGNR doped with SO_2 molecules were investigated for their electronic and mobility characteristics.
- Upon SO_2 adsorption, Cr-doped AGNR exhibited a significant change in electronic properties.
- Transducers and pressure gauges using the design were developed immediately.
- Sensors for more complex three-dimensional deformations can be developed based on this study.

1. Introduction

In recent years, nanotechnology has led to the development of electrodes that depend on nanomaterials with improved selectivity, sensitivity, and stability [1, 2]. Nanomaterials can be used to modify and functionalize electrodic surfaces to enhance their electrochemical signal, thereby makingit possible to develop sensors with high sensitivity and selectivity [3]. Electrochemical sensors based on nanomaterials have tremendous potential in many fields, including environmental monitoring, food safety, forensic analysis, and biomedical applications [4, 5]. Several advantages have been found in using nanomaterials in electrochemical sensors, including enhanced interfacial adsorption, improved electrocatalytic activity, biocompatibility, and faster electron transfer kinetics, all of whichhave increased selectivity and sensitivity toward detecting specific analytes, as well as improved overall performance [6-9]. These days, the excellent conductivity and fast electron transfer rates of carbon-based nanomaterials, such as graphene nanoribbons and graphene flowers, have been used widely for electrochemical sensor fabrication [10-12].

However, the growth and development of the industry have led to the release of some toxic gases in regions that threaten human safety and well-being [13]. Sulfur dioxide (SO_2) is a massive toxic gas released from elemental sulfur combustion. Besides respiratory diseases and nervous problems, lung cancer is one of its most critical adverse effects [14, 15]. When SO_2 is combined with water, sulfuricacid is produced, which can cause death if overexposed to the eyes and skin [16]. Environmental gas sensors are vital for monitoring and investigating air and gas quality [17]. According to recent progressin industry and biomedicine, detecting and monitoring toxic gases, even at low levels, has become a key to protection and environmental monitoring [18-20].

Several techniques for detecting lung cancer have been developed, like photon emission tomography (PET) [21], magnetic resonance imaging (MRI) [22], computed tomography (CT) [23], chest radiograph (CRG) [24], and X-ray method [25]. However, traditional techniques were notably limited in screening lung cancer in the initial stages. It was due to the low sensitivity to detect abnormal molecules, the price, and chemical destruction [26-28]. Different biosensors, such as

electrochemical biosensors, have been invented to identify lung cancer biomarkers [29]. Compared to conventional techniques, these biosensors show excellent sensibility, selectivity, confidence, low cost, and easy operation in complex representations [30]. Electrochemical biosensors, using an antibody as the bio- recognition agent, are also helpful for cancer biomarker detection [31]. Detection of biomarkers by immune-based biosensors is a promising technique because of their sensitivity and specificity [32-34].

Among the various nanomaterials, 2D nanomaterials have attracted significant attention due to their different structural dimensions [35]. The transport of charge carriers in heat makes 2D nanomaterials possess remarkable electrical properties [36]. Various combinations of elements and compounds comprise the family of 2D materials in the periodic table. In addition to metals, insulators,conductors, and semiconductors, a wide range of properties can be generated [37]. Two-dimensional materials are well-known for their layered structure with chemical solid interactions in planes and loose interactions between layers. As a result of this layered structure, the bulk counterpart is more likely to break up into individual and free atomic layers [38]. Also, 2D layered structure can be synthesized using film formation techniques, a fundamental part of the electronic industry [39]. Thus, 2D materials can be developed for nanoelectronics and flexible electronics [40, 41]. Due to graphene discovery, nanoelectronics applications grew, and many materials were included in the 2D family. A vital element of the ongoing technological advancement is the development of two-dimensional materials that are cost-effective and sustainable [42]. It is possible to reduce the surface energy of these materials by restructuring their high-density and unstable bonds. Studying two-dimensional layered materials, including MXenes and graphene, has become increasingly popular because they have two-dimensional properties [43]. Compared with bulk materials, two-dimensional materials play a crucial role due to their unique properties, including electron confinement, increased surface-to-volume ratio, and elimination of van-der Waals interactions [44]. Because of their nanosheet-like structure, MXenes and graphene exhibit exceptional conducting properties. Carbon atoms are tightly bound in hexagonalstructures in graphene, while MXenes are obtained by exfoliating different transition metals. Besides transistors and sensors, these materials are also suitable for

electrodes, supercapacitors, and photodetectors [45, 46].

In recent years, graphene nanostructures have become a focus of intense research due to their impressive properties and potential applications in novel electronic devices [47]. On the other hand, two-dimensional (2D) graphene is a semimetal, so its applications are limited. There is a chemical influence on graphene nanoribbons (GNRs) electronic characteristics depending on ribbon length and width [48]. According to research, graphene can detect various gases, but SO_2 molecules are weakly adsorbent to intrinsic graphene. In contrast, graphene-based chemical gas sensors for SO_2 can be improved by doping them with chromium (Cr) [49]. A recent study by Yu Li et al. reported that an electrode layer composed of AuNPs and enhanced graphene could generate an immunosensor (GR). An immunological component of the biosensor was a monoclonal antibody that captured CEA (anti-CEA), one of the recognizable cancer markers not only in lung cancer but also in breast and pancreatic cancers [50]. Zhang D,. et al. studied SO_2 adsorption on graphene oxide using density functional theory(DFT) calculations. As a result of SO_2 adsorption on GO, the electronic properties of GO sheets change, and charge redistribution occurs. Since GO has high sensitivity and response to SO_2, it may be a promising candidate for SO_2 sensing applications [51]. Li W. et al. used molecular dynamics calculations to study SO_2 adsorption on graphene oxide. This study analyzed adsorption energy, charge transfer, and structural changes in GO- SO_2 systems. Due to solid interactions between SO_2 molecules and oxygen-containing functional groups on GO, their findings suggest GO possesses high sensitivity and selectivity for SO_2 gas detection [52]. In a recent review, Qian L. et al. reported advancements in graphene oxide-based gas sensors, namely SO_2 detection. This review paper discusses the methods of fabricating GO-based sensors, their sensing mechanisms, and their performance properties. As a promising SO_2 detection material, GO is also highlighted in the review due to its large specific surface area, high gas adsorption capacity, and tunable properties [53]. Chen X-P. et al. investigated graphene oxide's gas-sensing properties for SO_2 detection; Wang used DFT calculations. A comparison of the adsorption energies and charge transfer between SO_2 and GO showed that GO can adsorb SO_2 molecules effectively. This study considers GO a potentially sensitive material for SO_2 detection [54]. They performed a first-principles calculation of graphene oxide's

gas-sensing properties for detecting SO_2. The GO- SO_2 system was examined for its adsorption energies, charge transfer, and electronic properties. Because SO_2 molecules and oxygen functional groups form a strong interaction,their results suggest GO's sensitivity and selectivity for SO_2 detection [54].

Analyzing and optimizing the detection process relies heavily on the simulation method. There are several reasons for using graphene oxide in the simulation method for SO_2 gas detection such as: Sensitivity: Graphene oxide has a very high surface-to-volume ratio, which allows it to interact effectively with gas molecules. Simulation methods allow us to understand graphene oxide's interaction with SO_2 at the atomic and molecular level. In this way, sensors can be designed to detect even trace amounts of SO_2 with an increased sensitivity. Optimization: Simulation methods can provide insight into the properties of graphene oxide-based sensors and explore and optimize their structural and chemical properties. Simulators can determine graphene sensor characteristics, including response time, recovery time, and detection limit. Various attributes of these objects are manipulated, including their size, shape, defects, and functional groups. This optimization process can develop a highly efficient and reliable SO_2 gas sensor. Some authors explain the matter effectively here [55-58]. Based on DFT computations, Salih et al. analyzed graphene oxide's interactions with SO_2, CO_2, and CO gases. They investigated adsorption energies, charge transfer, and electronic propertiesto understand how sensing processes work [14]. The adsorption of SO_2 gas onto graphene oxide is alsoinvestigated by Chen et al. using DFT calculations. This study aimed to conceptualize the connection between SO_2 and graphene oxide by investigating the adsorption structures, binding energies, and charge transfer [59]. Li et al. studied SO_2 gas sensing theoretically using graphene oxide via DFT calculations. This research aims to study the binding energies, electronic characteristics, and charge transfer processes of graphene oxide towards SO_2 [60].

In our method, we have used the first strategy to analyze the spin-dependent electronic properties of undoped zigzag graphene nanoribbons (ZGNR), armchair graphene nanoribbons (AGNRs), Cr-doped ZGNR, and Cr-doped AGNR before and after reacting with SO_2 molecules to evaluate the

potential of ZGNRs as gas sensors. Several Cr atomic positions are analyzed in ZGNRs, AGNRs, and over magnetic boundary states based on adsorption energies, charge transfers, density of states, transmission spectra, I–V characteristics, and the molecular projected self-consistent Hamiltonian (MPSH). The results of this study may provide insight into the electron transport properties of graphene, which may lead to high-performance graphene sensors. Gas sensing is the topic of this paper, and it proposes ways to improve it. In this way, graphene-based chemical gas sensors that detect SO_2 can significantly enhance their sensitivity. Theoretically, this paper explores the possibility of doping AGNR and ZGNR with Cr to improve their ability to detect SO_2 gas. We have calculated DFT using Atomistix Toolkit Virtual Nanolab (ATK-VNL) and MATLAB to simulate and synthesize our algorithm. The electronic structure is sensitive to the gases' adsorption and could be a charge donor or acceptor of graphene. Accordingly, the absorption rate of gases is compared and simulated using AGNR and ZGNR and applying SO_2 gas properties. Compared to existing SO_2 detection technologies, such as metal oxide and electrochemical sensors, Cr-doped GNRs offer theoretical advantages in sensitivity and selectivity. Our simulations indicate that these sensors could achieve rapid response times and detect low concentrations of SO_2, outperforming current methods. However, challenges such as interference from other gases and ensuring long-term stability must be addressed in practical implementations.

2. Computational Methods and Analysis

This study has utilized DFT as implemented in Atomistix ToolKit (ATK) to analyze the electronic properties, adsorption energy, and density of states (DOS) of GNRs before and after SO_2 exposure. The Generalized Gradient Approximation (GGA) with the Perdew-Burke-Ernzerhof (PBE) exchange-correlation function is employed to capture the electronic interactions within the system. The PBE functional is known for providing a good balance between computational efficiency and accuracy for systems involving adsorption processes and spin-polarized calculations, which are central to our analysis of the spin-dependent electronic properties of both undoped and Cr-doped

ZGNRs and AGNRs.

In the current method, two different cut-off energies are employed for various aspects of the calculations:

1) *400 eV Cut-off Energy*: For electron-ion interaction simulations, we have used a higher cut-off of 400 eV in the projector-augmented wave (PAW) method. This value defines the energy threshold above which plane waves are excluded from the basis set, ensuring accurate modeling of the electron-ion interactions while balancing computational cost. The number of electronic steps is automatically determined by the software to ensure accurate convergence of the electronic structure calculations. This energy threshold defines the maximum kinetic energy of plane waves included in the basis set, balancing accuracy and computational cost. This approach also ensures accurate modeling of electron-ion interactions while effectively managing computational resources [61].

2) *150 Ry Cut-off Energy*: The 150 Ry (Rydberg) cut-off energy is used in the context of the non-equilibrium Green's function (NEGF) formalism implemented in ATK. This cut-off energy applies to the double-zeta polarized (DZP) basis sets for electronic structure calculations, particularly for the two probe systems that study electron transport properties. This approach enabled accurate modeling of electron behavior under bias voltage, specifically for Cr-doped and SO_2-adsorbed GNRs. The NEGF formalism is essential for calculating the I-V characteristics, transmission spectra, and electronic conductance of the nanoribbons, offering valuable insights into their potential as SO_2 gas sensors. The 150 Ry energy cut-off defines the maximum kinetic energy of plane waves included in the basis set, striking a balance between accuracy and computational efficiency [62].

Journal Pre-proof

2.1. Materials Synthesis and Sensor Fabrication

The synthesis of Cr-doped GNRs with precise doping levels is crucial for achieving optimal sensor properties. Techniques such as chemical vapor deposition (CVD) and molecular beam epitaxy (MBE) can be adapted to produce high-quality GNRs with uniform Cr doping [63]. Additionally, integrating these GNRs into sensor devices necessitates careful consideration of fabrication methods to ensure scalability to industrial production while maintaining performance and stability.

For the Brillouin-Zone (BZ) optimization in our simulations, a k-point grid of 1×1×10 is used, with the z-direction aligned along the ZGNR growth direction. This sampling choice is crucial for precise calculations of electronic structure, band structure, and density of states. Specifically, the 1×1×10 grid means:

- 1 point in the x-direction
- 1 point in the y-direction
- 10 points in the z-direction (length of the nanoribbon)

A vacuum pad greater than 10 Å is employed in the *x* and *y* directions to minimize interactions between periodic images, and the energy balance threshold is set to 0.03 eV/Å. Effective BZ optimization ensures accurate and efficient simulations, capturing essential features of the electronic structure and verifying the stability and reliability of results. It is particularly important for applications in sensors, electronic devices, and other technologies. According to this definition, Eq. (1) calculates the adsorption energy.

$$E_{ad} = E_{sheet} + E_{SO_2} - E_{total} \quad (1)$$

where E_{ad} is the adsorption energy, E_{sheet}, E_{SO_2}, and E_{total} are the energies of the isolated graphene sheet, the isolated SO_2 molecule, and the relaxed graphene sheet with an adsorbed SO_2 molecule, respectively.

Double-Zeta Polarized (DZP) basis sets are employed for both geometric optimizations and transport calculations to enhance the accuracy of electronic structure analyses. The DZP basis sets use two basis functions per atomic orbital and include polarization functions, enabling the detailed capture of electronic interactions and bonding characteristics [64]. It makes DZP particularly suitable forthe complex systems analyzed using DFT and NEGF approaches.

Geometry optimization was performed with a force tolerance of 0.05 eV/Å, which sets the criterion for the precise adjustment of atomic positions. This tolerance represents the maximum allowable force on any atom before the geometry is considered converged, ensuring minimized forces and accurate atomic configurations. The chosen tolerance strikes a balance between precision and computational efficiency, preventing unnecessary computational costs while maintaining accuracy. By setting the force tolerance at 0.05 eV/Å, the geometries of the graphene nanoribbons (ZGNR and AGNR) and the adsorbed SO_2 molecules were effectively relaxed, leading to reliable electronic structure calculations and energetically stable configurations.

Additionally, k-point sampling was performed in the x, y, and z directions to represent the electronic structure across the entire Brillouin zone accurately.

According to the Landauer-Büttiker formula, the current can be calculated as follows:

$$I = \frac{2e}{h} \int_{-V/2}^{V/2} T(E,V) dE. \quad (2)$$

[-V/2, V/2] specifies the bias window region, and T (E, V) indicates the bias-dependent transmission coefficient. The model systems examined in this study can be seen in Fig. 1. These systems contain five ZGNR lines, 11 dimer carbon atom lines, and monoatomic hydrogen along their edges. Our model is based on a supercell with 11 dimer lines to account for adsorption and impurities. A single SO2 molecule is adsorbed to the doped Cr atom in this system, substituting for a C atom. We investigated five different Cr doping sites (labeled 1-5 in Fig. 1 from edge to center). According to Cr location, ZGNR with Cr at site one is called Cr1-ZGNR, etc. Each ZGNR-based device includes an absorbing area and two non-overlapping electrodes (left and right). Electrodes and dispersion areas have the same diameter.

2.2. Electronic and Magnetic Properties

The magnetic moment induced by Cr-doping in GNRs is crucial in determining their spin-dependent electronic properties. Specifically, the magnetic moment of 3.0 μB in Cr-doped ZGNRs and 2.5–3.0 μB in Cr-doped AGNRs significantly influences the spin polarization within the nanoribbons. In this sudy, we have performed spin-polarized DFT calculations to accurately capture the magnetic properties of Cr-doped GNRs. The calculations are set up to allow for spin degrees of freedom, ensuring that both spin-up and spin-down electrons are treated separately.

This spin polarization directly affects the electronic structure, leading to distinct spin channels that can be exploited in spintronic devices. A robust magnetic moment suggests that Cr-doped GNRs could exhibit enhanced sensitivity to external perturbations, such as gas adsorption, due to the interplay between spin and charge transport mechanisms.

In gas sensing, the magnetic moment enhances the interaction between the GNRs and gas molecules like SO_2. The spin-dependent electronic states created by the Cr dopants can lead to different adsorption energies and charge transfer dynamics for various spin orientations. It, in turn, affects the conductivity and current response of the GNRs, providing a more pronounced and detectable signal when exposed to the target gas.

The significant I–V difference observed with and without SO2 adsorption in Cr-doped ZGNRs can be attributed to these spin-dependent interactions. The magnetic moment, therefore, contributes to the intrinsic magnetic properties of the GNRs but also enhances their functionality as sensitive and selective molecular sensors.

This understanding of the magnetic moment's role underscores the potential of Cr-doped GNRs in spintronic applications and as high-performance components in graphene-based gas sensors, particularly for detecting gases like SO_2.

The spin-dependent overall energies *E* are calculated for the five different doping locations (1-5) in ZGNR (Fig. 1a). Cr is found to preferentially adhere to the edge of ZGNR, with site one being the stickiest due to the element's affinity. This behavior can be attributed to hydrogen's lower electronegativity than carbon, resulting in a more vital Cr–Hydrogen (H) bond than the Cr–C bond. Like nitrogen (N) and boron (B), Cr–H bonds exhibit greater strength than Cr–C bonds. For this discussion, the focus will be on Cr1-ZGNR. In addition to the varying Cr doping sites, different magnetic phases also play a role in determining model reliability. The objective is to identify the most stable magnetic phase among pure ZGNR, SO_2+ZGNR, Cr1-ZGNR, and SO_2+Cr1-ZGNR, considering nonmagnetic (NM), ferromagnetic (FM), and antiferromagnetic (AFM) phases.

A graphene system contains a central structure attached to a nanoribbon that acts as a sensor. This structure comprises an exposed graphene quantum ring surrounded by SO_2 molecules positioned along the magnetic field's z-axis and the electric field's x-axis. A graphene quantum ring consists of rows of carbon atoms (atom chains) arranged in a hexagonal shape. SO_2 gas molecules are absorbed at selected sites.

GNR is classified into zigzag and armchair graphene nanoribbons based on how the carbon

atoms are arranged at the corners [65]. The research used graphene-nanosheet, armchair graphene-nanoribbon, and zigzag graphene-nanoribbon to identify SO_2 gas. As a result of binding energies, densities of states, and band structures, the electronic properties of the adsorption system have been investigated [65]. Fig. 1 shows the ZGNR and AGNR sensor's atomic structure. 5-ZGNR is as wide asfive carbon atoms. The edges are saturated with hydrogen atoms to absorb SO_2 gas molecules better.

Recently, nanocarbons, GNRs, and nanometer-wide graphene stripes have attracted increasing attention for their interesting physical properties. One of the most attractive properties of GNRs is their tunable electronic and magnetic characteristics through the qualification of the nanoribbon's width and edge geometry. Therefore, a simple and effective method must be developed to create GNRs at bulk scale with atomic precision and for future application in logic design. In a molecular sense, perylene (PER) is a precursor to an armchair-type GNR with five carbon atoms in cross-section (AGNR). AGNR can be produced from monomers by on-surface polymerization and reinforced with crystalline metal surfaces in the coupling process. Fig. 1b shows the armchair sensor's atomic arrangement. Cr is injected as an impurity into the structure to improve the sensor’s electronic properties.

Journal Pre-proof

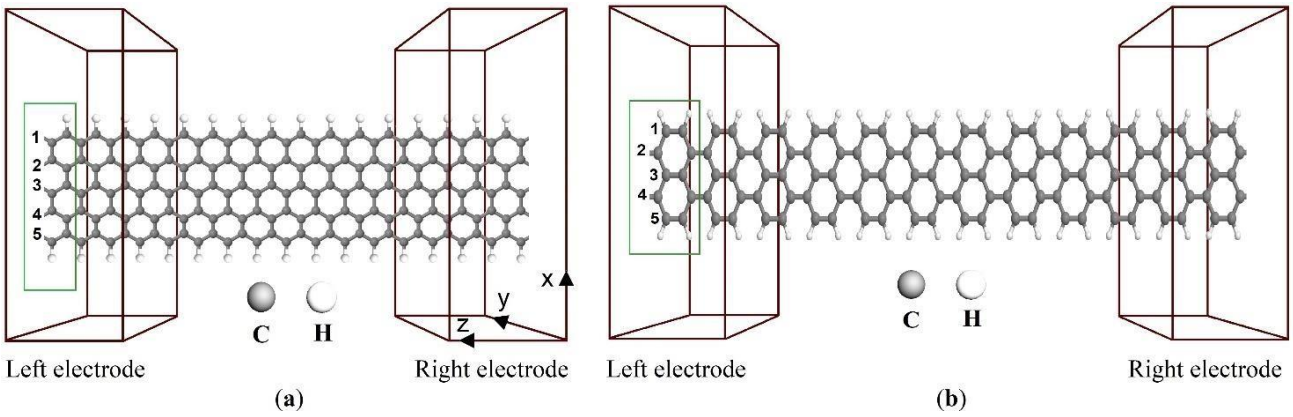


Figure 1. Atomic structure (**a**) ZGNR and (**b**) AGNR. The gray and white balls correspond to carbon and hydrogen atoms, respectively and the prime cell of GNR is marked by the green squareframe.

As shown in Fig. 2, a doped Cr atom replaces a C atom in this system with an adsorbed SO_2 molecule. In this study, five distinct spots for Cr doping were analyzed. Any ZGNR-based device consists of three distinct regions: an emitting region and two semi-infinite electrodes (right electrodeand left electrode). These electrodes can be made of metal, graphene, or carbon nanotubes. In addition, the electrodes in the nanoribbon, for example, can be made of metal, gold, platinum, or graphene. This paper employed graphene electrodes. It should be noted that both the emission regionand electrodes have the same width.

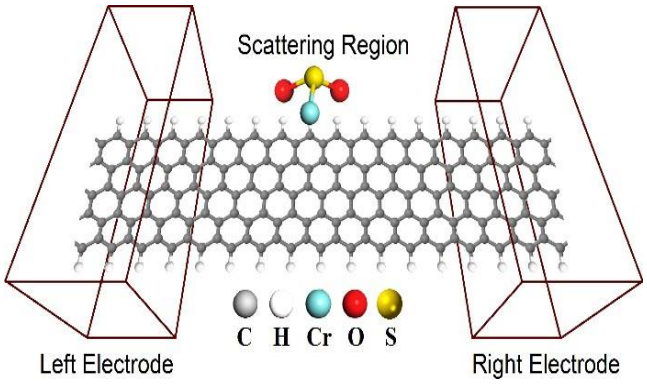


Figure 2. Schematic diagram of a ZGNR two-probe system with an adsorbed SO_2 molecule and one Cr atom substituted.

3. Results and Discussion

An adsorption structure with various initial directions and locations is designed to investigate the reaction process of SO_2 on pristine graphene layers. The ideal adsorption structure can be determined by analyzing the dimensions and energies of adsorption. In addition, it considers the difference between the current and voltage curves. As a result of the absorption process, pristine graphene changes its electrical properties. Eq. (3) gives the energy gap (Eg) between lowest unoccupied molecular orbital (LUMO) and highest occupied molecular orbital (HOMO), where E_{LUMO} and E_{HOMO} describe the deepest unsaturated molecular orbit and the largest saturated molecular orbit.

$$E_g = \left| E_{LUMO} - E_{HOMO} \right| \tag{3}$$

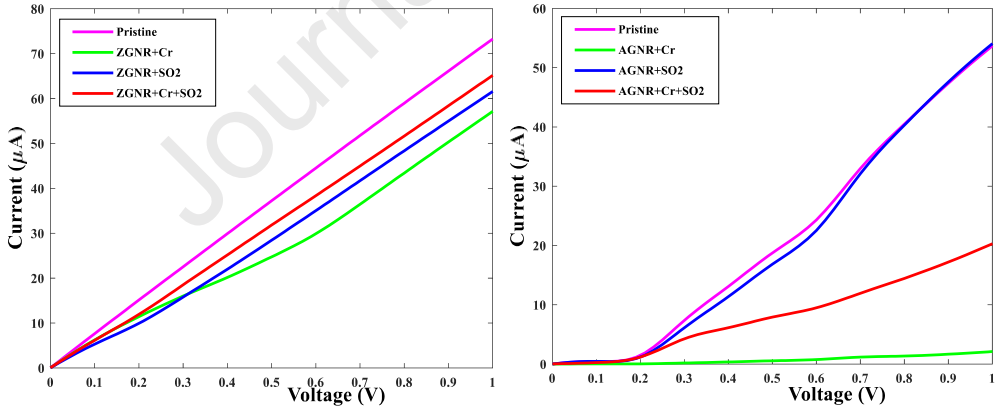
Shao et al. [66] used the DFT method to study the effects of SO_2 molecules on the geometrical structures and transport properties of pure and Cr-doped 5-ZGNR. According to their findings, edgedoping in 5-ZGNR is the most advantageous configuration. In contrast to pure ZGNR, Cr-doped ZGNR absorbed SO_2 more strongly. According to their study, significant uninterrupted transmission channels exist as energy passes through the transmission gap. The I–V characteristics for their models in ZGNR had semiconductor properties, and the threshold voltage was around 0.3V. The I–V curves are sharply curved at charges higher than the threshold voltage. In the areas above the threshold bias, the current will increase proportionally to the extent of rising. This is because the electrons in the valence band in an electrode can pass through the tunneling band and be transmitted through the center to the conduction band.

On the other hand, when the charge is applied to Cr1-ZGNR and SO_2+Cr1-ZGNR, the currents begin to rise. Despite this, distinctions between the two curves can be detected.

When the bias is more significant than 0.25V, the assessed value of Cr1-ZGNR is about half of the value of SO_2+Cr1-ZGNR below the same bias.

Due to the similarity of the currents for ZGNR and SO_2+ZGNR, we can predict that ZGNR isunsuitable for detecting SO_2 gas. As a result of its doping, its transport properties are crucial. The notable I-V difference between Cr1-ZGNR with and without SO_2 adsorption is consistent with its potential as a molecular sensor.

Fig. 3 shows the current-voltage characteristics of the mentioned states in ZGNR and AGNR.In Fig. 3a, the graph is a straight line in the pristine state with a maximum voltage of 1V for ZGNR state. Despite this, the current changes significantly when SO_2 molecules are absorbed. These changescan be used to detect SO_2 molecules. An impurity like Cr reduces the current by 1v, while a moleculelike SO_2 and an impurity like Cr generate a more linear absorption.



(a) (b)

Figure 3. The I–V characteristic for the different states (**a**) ZGNR and (b) AGNR. (a) The I–V characteristic includes pristine, the addition of Cr and SO_2 gas in ZGNR. (**b**) variation of the current and voltage value for the different states, containing pristine, the addition of Cr and SO_2 gasin AGNR.

The current-voltage characteristics of AGNR are shown in Fig. 3b. The current is more potentin pristine states than in others. Injecting Cr impurity significantly reduces this

gap. The changes arestrongly observed when an impurity is injected, and a gas molecule is absorbed. In this situation, gascan be detected by considering the difference between the states when the sensor displays a bias undera fixed voltage. The injected impurity in AGNR reduces the current gap and enhances the sensor's sensitivity to detect gas molecules. By monitoring the changes in current under a fixed voltage, the presence of gas can be accurately detected, making the injected impurity a crucial component in gas- sensing applications.

Fig. 4 shows the different states between ZGNR and AGNR, including pristine, added Cr, and SO_2 gas in Figs. 3a and 3b. It should be noted that the output current changes for any extra molecules.These changes are indications that a gas molecule has been added to graphene nanoribbons. Unwantedgases can be detected by considering the potential difference between the pristine state and when gasmolecules such as SO_2 are present. It is easy to recognize the differences between various states from 0.2v to 1v in Fig. 3a. But in Shao et al.'s method [66] , we cannot observe any changes in the SO_2+ZGNRstate. It confirms that observation of gas molecules is possible at low density.

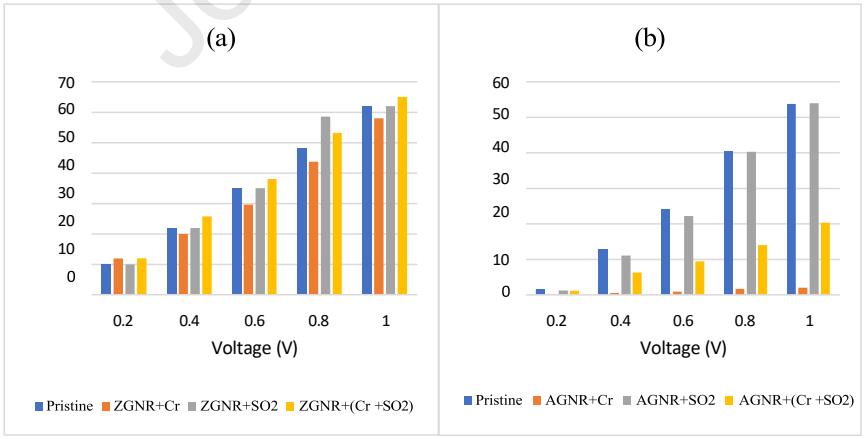


Figure 4. The comparison of the different states including pristine, the addition of Cr, and the addition of SO_2 gas in Figs. 3a and 3b. (**a**) shows the rate of variactios in Fig. 3a. in different states. (**b**) shows the rate of variactios in Fig. 3b in different states.

Fig. 4b shows the different states, including the pristine state and the addition of Cr

and SO_2 gas, as represented in Fig. 3b. Notably, each molecule has another output current. These changes indicate that a gas molecule has been added to graphene nanoribbons. Considering the differences inthe current in the pristine state and after adding gas molecules such as SO_2, one can observe the number of unwanted gases. On the other hand, the changes in the current observed in graphene nanoribbons after introducing gas molecules, such as SO_2, indicate that the presence of these molecules affects the material's conductivity. The different output currents suggest that gas moleculesinteract with graphene nanoribbons, altering their electronic properties. It leads to variations in electric charge flow.

Table 1 compares the output currents for Shao et al.'s method [66] and Fig. 3a in the SO_2+Cr state. As the sensor sensitivity increases, the output current and voltage difference becomes more significant. Hence, it is the clear state observed in Table 1. For instance, when Vin =0.3v, Iout in Shao et al.'s method [66] is 15.6 (μA), but we can improve the output current rate in Fig. 3a to 18.8 (μA). It shows that the difference between V and I_{out} has increased, which impacts the sensor's sensitivity. Our main goal is to enhance sensation. According to Shao et al.'s study [66], when Vin is 0.5v, the I-V curve difference has reached its maximum rate, and the output current value is lower than the output current. The comparison between the output current values in Shao et al.'s method [66] and Fig. 3a for different Vin values in Table 1 highlights the sensor's increased sensitivity in the transparent state. As the difference between Vin and Iout increases, the sensor's sensitivity improves,with Fig. 3a exhibiting higher output current rates than Shao et al.'s method [66], mainly when Vin is 0.3v and 0.5v. This finding is consistent with previous research conducted by Shao et al. (2014) [66] , which demonstrated that increasing the difference between the input voltage and the output current results in a higher sensor sensitivity. The study concluded that this enhanced sensitivity is crucial for accurate and reliable detection of target substances in various applications.

Table 1. Comparison of the output currents for Shao et al. (2014) [66] and Fig. 3a in SO_2+Cr state.

	Shao et al. [66]	Fig. 3a
Vin (v)	Iout (μA)	I(μA)
0.3	15.6	18.8
0.4	20.1	25
0.5	25.3	32

ZGNR did not differ much between pristine and added impurity states in Fig. 3a. However, Fig. 3b indicated that the current difference is more pronounced in AGNR than in ZGNR. Further details for comparing the difference between sensor output currents in Fig. 3a and Fig. 3b are shownin Table 2. Based on Table 2, we can find the difference rate between the following Eq. (4) and Eq. (5).

Eq. (4) describes the difference in Iout between a pristine zigzag graphene nanoribbon (ZGNR) and a ZGNR doped with Cr and exposed to SO_2 gas. Here, IPristine represents the output current of the undoped ZGNR, while I_(ZGNR+Cr+SO_2) indicates the output current when the ZGNRis doped with Cr and has SO_2 adsorbed on its surface. This equation captures the change in current resulting from the combined effects of Cr doping and SO_2 adsorption in the ZGNR.

$$I_{\text{out (Fig.5)}} = I_{\text{Pristine}} - I_{(ZGNR+C_r+SO_2)} \quad (4)$$

Similarly, Eq. (5) quantifies the difference in Iout between a pristine armchair graphene nanoribbon (AGNR) and an AGNR under the same conditions. IPristine refers to the output current of the undoped AGNR, while I_(AGNR+Cr+SO_2) measures the output current of the AGNR when doped with Cr and exposed to SO_2. It allows us to understand the impact of Cr doping and SO_2 adsorption on the AGNR's current.

$$I_{\text{out (Fig.6)}} = I_{\text{Pristine}} - I_{(AGNR+C_r+SO_2)} \tag{5}$$

By comparing the results from Eqs (4) and (5), the sensitivity of ZGNRs and AGNRs to SO_2can be assessed, allowing for the determination of which configuration is more effective as a gas sensor. For instance, when the input voltage (Vin) is set to 1 V, the output current difference (Iout) forZGNRs (Fig. 3a) is -4.1 μA, while for AGNRs (Fig. 3b), it is 32.62 μA. This substantial variation highlights that AGNRs, with their distinct electronic and magnetic properties, are more sensitive to Cr doping and SO_2 adsorption, making them more suitable for gas sensing applications.

Moreover, Eqs. (4) and (5) quantify the change in output current (Iout) between pristine graphene nanoribbons (GNRs) and those doped with chromium (Cr) and exposed to sulfur dioxide (SO_2). These equations are crucial for understanding how Cr doping and SO_2 adsorption influence the electrical properties of the nanoribbons, which is essential for evaluating their effectiveness as gas sensors.

Table 2. The biosensor's output currents differ in output current in equations (4) and (5).

	Fig. 3a	Fig. 3b
Vin (v)	Iout (μA)	Iout (μA)
0.2	-2	0.2
0.4	-3.7	7.05
0.6	-3	14.75
0.8	-5.23	25.5
1	-4.1	32.62

Journal Pre-proof

Guo et al.[67] presented a highly effective method for detecting gaseous SO_2 using differential resistivity measurements. This method, which involves examining the asymmetric current vs. voltage (I-V) characteristics, the adsorption energies, band structures, and the adsorption amount, demonstrated that GeSe monolayers along the zigzag direction are significantly more effective for SO_2 gas sensing compared to those along the armchair direction. In a contrasting approach, we used the DFT method to analyze the spin-dependent electronic behavior of undoped ZGNRs, AGNRs, Cr-doped ZGNRs, and Cr-doped AGNRs before and after absorbing SO_2 molecules, aiming to determine their suitability for gas sensors.

In Guo et al.'s method, the voltage increases sharply in the scattering region as the bias voltage rises from zero to 1.2 V, reaching a maximum value of 385.6 nA after SO_2 adsorption.

Nevertheless, as the bias voltage rises, the current drops rapidly and falls to a minimum of 2.6 nA at 1.3 V; an apparent negative differential resistance (NDR) behavior is visible. The calculated peak-to-valley ratio (PVR) for the current is 148.3. However, the PVR for the SO_2–GeSe in the armchair position is two orders lower than that for the device along the zigzag path.

In contrast, using the DFT method, Fig. 3a shows the I-V characteristics with and without SO_2 molecules in ZGNR. The scattering region current rose smartly when the bias voltage was raised from zero to 1.0 V. It reached a maximum value of 620 nA after SO_2 adsorption. It shows that in our method, the number of current changes in the ZGNR state is much more significant than in the GeSe method [67], and the detection sensitivity of graphene sensors is much higher than in other methods. Fig. 3b shows the I-V characteristics with and without SO_2 molecules in AGNR. The scattering region current increased when the bias voltage was raised from zero to 0.2 V. It reached a maximum value of 530 nA after SO_2 adsorption. The results indicate that our method's current change is significantly higher than the GeSe method after SO_2 adsorption. It suggests that graphene sensors based on ZGNR and AGNR exhibit better detection sensitivity towards SO_2 molecules than those found on ZGNR and AGNR in the GeSe method.

The difference between the sensor's output currents in ZGNR and AGNR states helped us understand that the potential difference in the AGNR state is more excellent than both ZGNR and the

pristine state. Hence, the higher AGNR sensor sensitivity. These two types also differ because Armchair graphene nanoribbon (AGNR) could neutralize the sensor, showing approximately zero current in the range of 0 to 0.2V (Fig. 3b). However, the ZGNR increased from the start. It may be due to the noise of the surrounding currents or other noises. These explanations reveal that AGNR can be controlled and produces less noise than ZGNR.

Fig. 5a shows the transmission spectra of energy for various states in ZGNR: no added impurity, added Cr impurity, and SO_2 molecule absorption. In the case of added Cr impurity, the passing graph shows that the most diminutive passage belongs to Cr. Current is directly related to the volume of the current pass, which means that a minor pass leads to a smaller current than in other states.

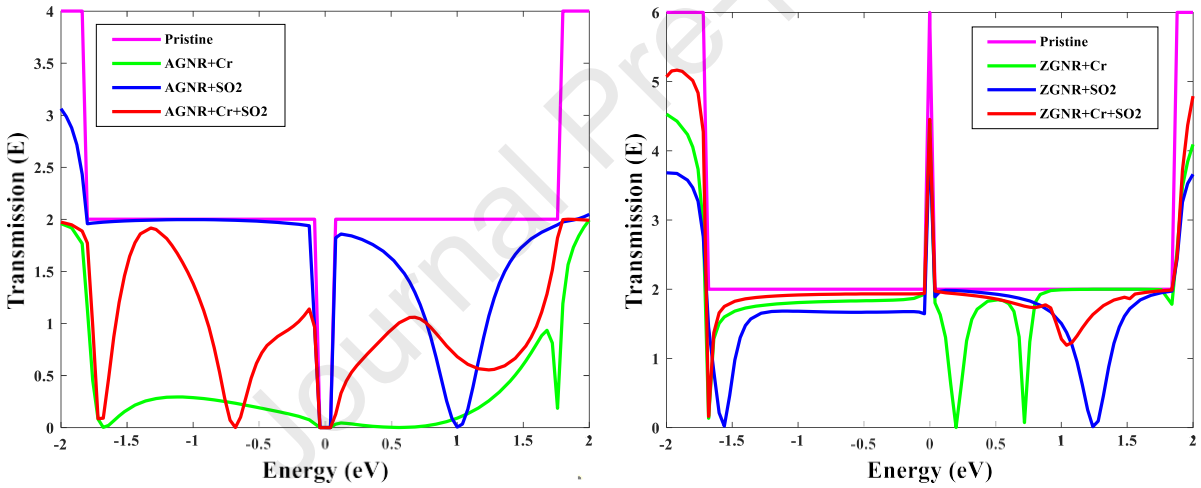


Figure 5. Transmission spectra in terms of energy for (**a)** ZGNR and (**b**) AGNR states, includingpristine, the addition of Cr and SO_2 gas.

Fig. 5b shows the transmission spectra in terms of energy for various states in AGNR. In this case, the transmission rate of added Cr impurity is much lower than in ZGNR states, thus reducing the volume of the corresponding current. Unlike the zigzag (ZGNR) sensor, this type of sensor requires a degree of bias to conduct the current. This bias is called the threshold voltage, which is approximately 0.2V. This amount of bias facilitates a noise-less sensor and enables its calibration. Unlike the zigzag (ZGNR) sensor, which allows for a higher transmission rate of added Cr impurity

and a larger corresponding current volume, this type of sensor requires a threshold voltage of approximately 0.2V to conduct the current. This lower transmission rate and the need for bias contribute to a quieter, more calibrated sensor, ensuring accurate measurements and reducingpotential noise interference.

Fig. 6a is a graph of the density of states in terms of energy in different ZGNR states. It is possible to observe that the number of states changes for some energy values. The most sensitive point is the Fermi level. In our DFT calculations using ATK, we have employed Fermi-Dirac smearing with a smearing width ranging between 0.07 and 0.55 eV. This range was chosen to optimize the convergence of electronic states near the Fermi level across different simulations, balancing accuracy in occupation states with computational stability.The number of electrons decreases in the added impurity state, and gas molecules are absorbed compared to the no-added impurity state.

According to Guo et al.'s method, systems based on pristine monolayer GeSe and SO_2–GeSe during the zigzag direction have different DOS. A partial DOS of SO_2–GeSe shows the lone impurity state at about 0.4 eV. It is equivalent to the device DOS of a pure GeSe monolayer, which results in the appearance of the lone impurity state. In contrast, Fig. 6a shows that the difference between the curve peaks in all cases is far more than the GeSe method. In our method,the density of states in ZGNR states exhibits variations for different energy values, with the most significant change occurring at the Fermi level. The number of states decreases in the added impurity state, indicating a lower electron count and the absorption of gas molecules, in contrast to the no-added impurity state. It suggests that the presence of impurities in the ZGNR affects the energy distribution of the system, leading to altered electronic properties and potential applications in sensing and gas absorption.

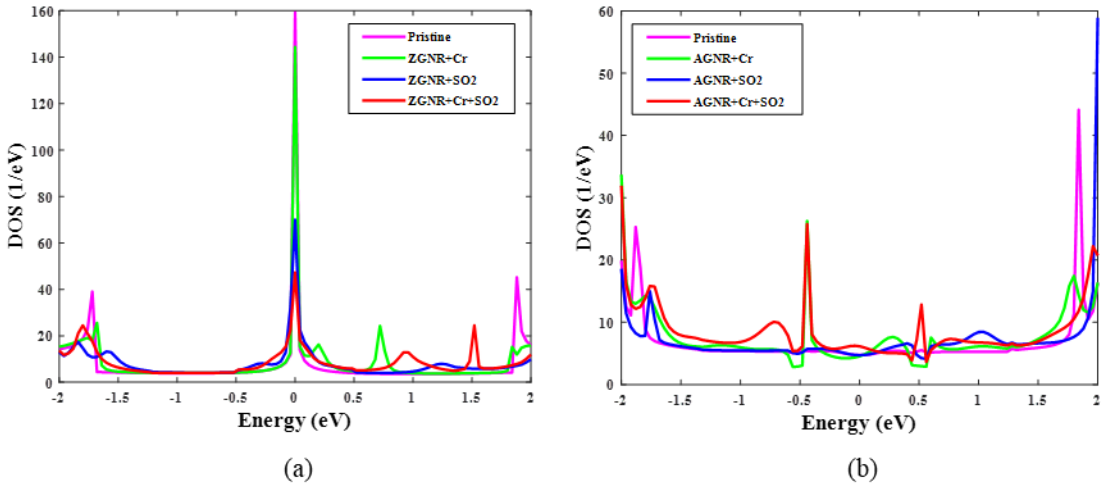


Figure 6. Graph of the density of states in terms of energy for various states, including pristine, theaddition of Cr and SO_2 gas in ZGNR (**a**) and AGNR (**b**)

A graph of state density based on energy is shown in Fig. 6b. In the case of injecting Cr and SO_2, an increase in the curve is observed (approximately -0.5 eV). As a result, Cr contains orbitals that increase the number of electrons in its valence band. Comparing pristine AGNR with ZGNR, pristine AGNR exhibits the highest peak-level intensity. The higher peak-level intensity in pristine AGNR can be attributed to several factors:

1. Pristine AGNR has a narrower bandgap than ZGNR, allowing for a higher concentration of electrons in its valence band.
2. The absence of impurities or defects in pristine AGNR ensures a more efficient and uninterrupted flow of electrons, resulting in a higher intensity of the peak level.
3. The unique structural properties of pristine AGNR, such as its specific arrangement of atoms and bonding patterns, further contribute to the enhanced intensity observed in its state density graph.

However, when comparing the state density based on energy between pristine AGNR and ZGNR, it is evident that ZGNR shows a significant decrease in peak-level intensity, indicating a lower number of electrons in its valence band compared to pristine AGNR.

4. Band Structure

The density of states and band structure diagrams are two electronic characteristics of materials. The band structure diagram demonstrates the arrangement of energy levels in different regions of the Brillouin zone. To determine gas sensitivity, the band gap can be observed before and after gas adsorption[68, 69].

This diagram makes it possible to distinguish the material's energy gap and the type of material in terms of whether its band is direct or indirect. The density of states diagram displays the number of states allowed for electron placement in the valence and conduction bands. It also shows the material's energy gap. Fig. 7 shows a band structure diagram. Fig. 7a corresponds to the band structure without impurity injection, where the energy gap value is 0.07 electron volts (eV), and the graphene nanoribbon has quasi-metallic behavior. By injecting Cr into the nanoribbon, we can see that the levels are separated on the Fermi surface, and the forbidden band is formed, as shown in Fig. 7b. In this case, the energy gap is about 0.55 eV. In the absorption state of SO_2, the density of energy levels around the Fermi level has increased. It is due to S and P orbitals in SO_2.

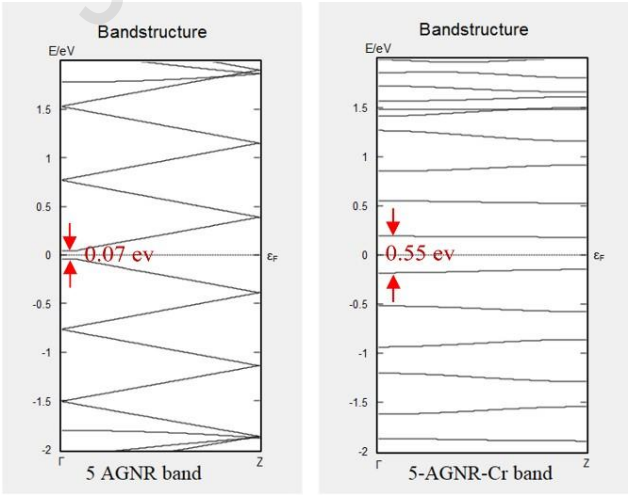


Figure 7. Band structure of AGNR. (a) without impurity injection, (b) the injection of Cr and SO_2absorption.

It should be noted that graphene ribbons have optical potential, too. Ribbons must be placed

on an appropriate substrate and exposed to wave radiation. The reflected part can be treated as a sensing wave. Fig. 8 shows graphene ribbons on top of SO_2 coated with gold on the backside. Depending on the operational range, geometrical sizes must be changed. For instance, scaling a few µm for gold and oxide consistency is appropriate in the Terahertz (THz) gap. The point in the sensing process is that surrounding environments with and without toxic gases exhibit different refractive indices. Another view states that equivalent impedances can model each element in the device and the external environment. In this vision, comparing the surrounding environment and the entire structure can be used to predict the sensor behavior.

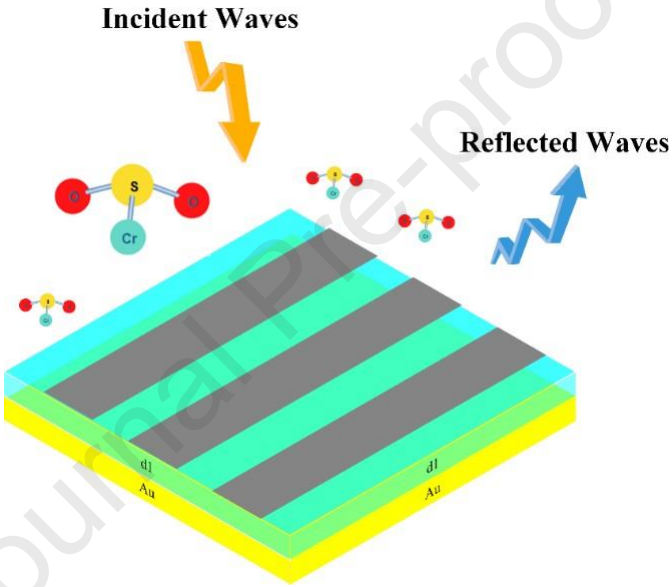


Figure 8. Graphene ribbons exploitation for optical sensing.

SO_2 detection using graphene ribbons based on optical reactions has been a subject of recent research, with various studies focusing on the enhancement of sensitivity and the underlying mechanisms. For instance, both nitrogen doping and blue-light irradiation were found to improve the sensitivity of graphene-based SO_2 sensors or *Pt* doping significantly enhanced the sensitivity of the sensors. Additionally, the gas sensing of graphene nanoribbons functionalized with different adsorbates, including CO, CO_2, and SO_2. As a direct result, adsorption energy and sensitivity of the nanoribbons varied depending on the adsorbate.

5. Summary and Conclusion

This study aimed to enhance SO_2 gas detection using graphene-based sensors, which have potential applications in lung cancer detection. The sensor was simulated with side electrodes to inject chromium (as an impurity) and sulfur dioxide, and its electronic properties were analyzed. The current-voltage characteristics indicate that the current volume is influenced by gas absorption and the type of gas molecule. As gas molecules pass through the sensor's electric field, the detection range increases.

The results showed that armchair graphene nanoribbons (AGNRs) performed more efficiently than zigzag graphene nanoribbons (ZGNRs) under different voltages. AGNRs exhibited better control with less noise compared to ZGNRs, whose states increased with voltage and noise. Comparing the output currents of ZGNR and AGNR, it was found that AGNRs provided a more significant potential difference, indicating higher sensitivity to SO_2. Therefore, AGNR sensors were identified as the most effective system for SO_2 gas detection, with optimal voltage and current characteristics.

This work also explored the electromechanical coupling in semiconducting structures, which has direct applications in developing pressure gauges and displacement transducers. Although initially phenomenological, the design incorporated quantum-mechanical principles of electron transport, laying the groundwork for future sensor development to address more complex deformations. Additionally, non-substituted GNRs synthesized in this study could find applications inheterogeneous catalysts, solid-state gas sensors, and heat transfer materials.

Our DFT and NEGF-based study suggests that Cr-doped graphene nanoribbons exhibit significant potential as SO_2 gas sensors due to their enhanced electronic properties upon SO_2 adsorption. However, future experimental studies are essential to validate these computational predictions. Techniques such as X-ray photoelectron spectroscopy (XPS) and Raman spectroscopy should be employed to confirm the adsorption energies and electronic changes observed. Additionally, sensor

performance under varying environmental conditions and SO_2 concentrations should be tested to assess real-world applicability. Finally, it is important to note the need for wet lab validation to enhance the credibility of these findings, as the current work is based on simulations.

Author contribution statement

All authors made substantial contributions to the conception and design, acquisition of data, or analysis and interpretation of data; took part in drafting the article for important intellectual content; and agreed to be accountable for all aspects of the work.

Notes

The authors declare no competing financial interest

Data availability statement

Data will be made available in a repository on acceptance.

Acknowledgment

This research was supported by the Brain Pool program funded by the Ministry of Science and ICT through the National Research Foundation of Korea (Grant Number: 2022H1D3A2A02085952). This research was also supported by the National Research Foundation of Korea (NRF) grant funded by the Korean government (MSIT) (No. 2022M3J7A1062940 and RS-2023-00240052).

Journal Pre-proof

References

[1] M. Alhammadi, S. Aliya, R. Umapathi, M.-H. Oh, and Y. S. Huh, "A simultaneous qualitative and quantitative lateral flow immunoassay for on-site and rapid detection of streptomycin in pig blood serum and urine," *Microchemical Journal,* vol. 195, p. 109427, 2023.

[2] K. S. Ranjith *et al.*, "Fluorescence light-up electrospun membrane incorporated with perovskite nanoclusters as a highly sensitive colorimetric probe for detection of amine vapors during food spoilage," *Sensors and Actuators B: Chemical,* vol. 384, p. 133622, 2023.

[3] M. Safarkhani *et al.*, "Nanomaterial-assisted wearable glucose biosensors for noninvasive real-time monitoring: Pioneering point-of-care and beyond," *Nano Materials Science,* 2023.

[4] M. K. Masud *et al.*, "Nanostructured mesoporous gold biosensor for microRNA detection at attomolar level," *Biosensors and Bioelectronics,* vol. 168, p. 112429, 2020.

[5] J. H. Kim *et al.*, "Harnessing protein sensing ability of electrochemical biosensors via a controlled peptide receptor–electrode interface," *Journal of Nanobiotechnology,* vol. 21, no. 1, p. 100, 2023.

[6] S. Hamzeh, H. Mahmoudi-Moghaddam, S. Zinatloo-Ajabshir, M. Amiri, and S. A. R. Nasab, "Eco-friendly synthesis of mesoporous praseodymium oxide nanoparticles for highly efficient electrochemical sensing of carmoisine in food samples," *Food Chemistry,* vol. 433, p. 137363, 2024.

[7] H. Karimi-Maleh *et al.*, "Recent developments in carbon nanomaterials-based electrochemical sensors for methyl parathion detection," *Journal of Food Measurement and Characterization,* vol. 17, no. 5, pp. 5371-5389, 2023.

[8] M. Negahdary *et al.*, "Recent electrochemical sensors and biosensors for toxic agents based on screen-printed electrodes equipped with nanomaterials," *Microchemical Journal,* vol. 185, p. 108281, 2023.

[9] G. Balkourani, A. Brouzgou, and P. Tsiakaras, "A review on recent advancements in electrochemical detection of dopamine using carbonaceous nanomaterials," *Carbon,* p. 118281, 2023.

[10] U. Rajaji *et al.*, "Graphene nanoribbons in electrochemical sensors and biosensors: a review," *Int. J. Electrochem. Sci,* vol. 13, no. 7, p. 6643, 2018.

[11] T. S. Martins, J. L. Bott-Neto, O. N. Oliveira Jr, and S. A. Machado, "based electrochemical sensors with reduced graphene nanoribbons for simultaneous detection of sulfamethoxazole and trimethoprim in water samples," *Journal of Electroanalytical Chemistry,* vol. 882, p. 114985, 2021.

[12] F. M. Zahed, B. Hatamluyi, and M. K. Bojdi, "A sensitive electrochemical sensor based on graphene quantum dots/hierarchical flower-like gold nanostructures for determination of cytostatic drug flutamide," *Materials Science and Engineering: B,* vol. 300, p. 117109, 2024.

[13] A. I. Ayesh, "H2S and SO2 adsorption on Cu doped MoSe2: DFT investigation," *Physics Letters A,* vol. 422, p. 127798, 2022.

[14] E. Salih and A. I. Ayesh, "CO, CO2, and SO2 detection based on functionalized graphene nanoribbons: First principles study," *Physica E: Low-dimensional Systems and Nanostructures,* vol. 123, p. 114220, 2020.

[15] S. Han, X. Yue, J. Wang, Y. Zhang, B. Wang, and X. Song, "A novel near-infrared ratiometric fluorescent probe for SO 2 detection with a large emission shift," *New Journal of Chemistry,* vol. 44, no. 11, pp. 4554-4557, 2020.

[16] S. Hooshmand *et al.*, "Wearable nano-based gas sensors for environmental monitoring and encountered challenges in optimization," *Sensors,* vol. 23, no. 20, p. 8648, 2023.

[17] D. J. Buckley, N. C. Black, E. G. Castanon, C. Melios, M. Hardman, and O. Kazakova, "Frontiers of graphene and 2D material-based gas sensors for environmental monitoring," *2D Materials,* vol. 7, no. 3, p. 032002, 2020.

[18] D. Singh, M. Dahiya, R. Kumar, and C. Nanda, "Sensors and systems for air quality assessment monitoring and management: A review," *Journal of environmental management,* vol. 289, p. 112510, 2021.

[19] S. Uma and M. Shobana, "Metal oxide semiconductor gas sensors in clinical diagnosis and environmental monitoring," *Sensors and Actuators A: Physical,* vol. 349, p. 114044, 2023.

[20] Y. Yong *et al.*, "Highly sensitive and selective room-temperature gas sensors based on B6N6H6 monolayer for sensing SO2 and NH3: A first-principles study," *Results in Physics,* vol. 33, p. 105208, 2022.

[21] Y. Lei *et al.*, "Automated lung tumor delineation on positron emission tomography/computed tomography via a hybrid regional network," *Medical Physics,* vol. 50, no. 1, pp. 274-283, 2023.

[22] D. Zhu *et al.*, "Magnetic resonance imaging characteristics of brain metastases in small cell lung cancer," *Cancer Medicine,* 2023.

[23] W. K. Evans *et al.*, "Integrating Smoking Cessation Into Low-Dose Computed Tomography Lung Cancer Screening: Results of the Ontario, Canada Pilot," *Journal of Thoracic Oncology,* vol. 18, no. 10, pp. 1323-1333, 2023.

[24] S. H. Kwak, E.-K. Kim, M. H. Kim, E. H. Lee, and H. J. Shin, "Incidentally found resectable lung cancer with the usage of artificial intelligence on chest radiographs," *Plos one,* vol. 18, no. 3, p. e0281690, 2023.
[25] G. Dong *et al.*, "2D/3D Non-Rigid Image Registration via Two Orthogonal X-ray Projection Images for Lung Tumor Tracking," *Bioengineering,* vol. 10, no. 2, p. 144, 2023.
[26] A. Khodadoust, N. Nasirizadeh, S. M. Seyfati, R. A. Taheri, M. Ghanei, and H. Bagheri, "High-performance strategy for the construction of electrochemical biosensor for simultaneous detection of miRNA-141 and miRNA-21 as lung cancer biomarkers," *Talanta,* vol. 252, p. 123863, 2023.
[27] A. Khanmohammadi *et al.*, "Electrochemical biosensors for the detection of lung cancer biomarkers: A review," *Talanta,* vol. 206, p. 120251, 2020.
[28] V. M. Vijayan, L. Jothi, R. S. Arunagirinathan, and G. Nageswaran, "Recent advances in the electrochemical sensing of lung cancer biomarkers," *Biosensors and Bioelectronics: X,* vol. 12, p. 100235, 2022.
[29] H. Jiang, H. Zhang, M. Qin, M. Li, and X. Weng, "Ultrasensitive Sandwich-type Electrochemical Aptasensor for Dual Detection of Lung Cancer Biomarkers," *IEEE Sensors Journal,* 2023.
[30] L. P. Lin and M. T. T. Tan, "Biosensors for the detection of lung cancer biomarkers: A review on biomarkers, transducing techniques and recent graphene-based implementations," *Biosensors and Bioelectronics,* p. 115492, 2023.
[31] Y. Shoja, A. Kermanpur, and F. Karimzadeh, "Diagnosis of EGFR exon21 L858R point mutation as lung cancer biomarker by electrochemical DNA biosensor based on reduced graphene oxide/functionalized ordered mesoporous carbon/Ni-oxytetracycline metallopolymer nanoparticles modified pencil graphite electrode," *Biosensors and Bioelectronics,* vol. 113, pp. 108-115, 2018.
[32] R. Sheervalilou *et al.*, "Electrochemical nano-biosensors as novel approach for the detection of lung cancer-related MicroRNAs," *Current molecular medicine,* vol. 20, no. 1, pp. 13-35, 2020.
[33] L. K. Kiio *et al.*, "Development of electrochemical immunosensor for quantitative detection of non-small cell lung cancer (NSCLC) biomaker YES1," *Biosensors and Bioelectronics: X,* vol. 14, p. 100386, 2023.
[34] M. Chen, D. Wu, S. Tu, C. Yang, D. Chen, and Y. Xu, "A novel biosensor for the ultrasensitive detection of the lncRNA biomarker MALAT1 in non-small cell lung cancer," *Scientific Reports,* vol. 11, no. 1, p. 3666, 2021.
[35] M. R. Farani *et al.*, "2D MXene nanocomposites: electrochemical and biomedical applications," *Environmental Science: Nano,* 2022.
[36] J. N. Tiwari *et al.*, "Accelerated bone regeneration by two-photon photoactivated carbon nitride nanosheets," *ACS nano,* vol. 11, no. 1, pp. 742-751, 2017.
[37] J. N. Tiwari *et al.*, "Atomic layers of ruthenium oxide coupled with Mo2TiC2Tx MXene for exceptionally high catalytic activity toward water oxidation," *Applied Catalysis B: Environmental,* vol. 339, p. 123139, 2023.
[38] P. Kalambate *et al.*, "Progress, challenges, and opportunities of two-dimensional layered materials based electrochemical sensors and biosensors," *Materials Today Chemistry,* vol. 26, p. 101235, 2022.
[39] R.-E. Munteanu, P. S. Moreno, M. Bramini, and S. Gáspár, "2D materials in electrochemical sensors for in vitro or in vivo use," *Analytical and Bioanalytical Chemistry,* vol. 413, pp. 701-725, 2021.
[40] M. Varsha and G. Nageswaran, "2D layered metal organic framework nanosheets as an emerging platform for electrochemical sensing," *Journal of The Electrochemical Society,* vol. 167, no. 13, p. 136502, 2020.
[41] A. Aziz *et al.*, "Advancements in electrochemical sensing of hydrogen peroxide, glucose and dopamine by using 2D nanoarchitectures of layered double hydroxides or metal dichalcogenides. A review," *Microchimica Acta,* vol. 186, pp. 1-16, 2019.
[42] N. P. Shetti, D. S. Nayak, K. R. Reddy, and T. M. Aminabhvi, "Graphene–clay-based hybrid nanostructures for electrochemical sensors and biosensors," in *Graphene-based electrochemical sensors for biomolecules*: Elsevier, 2019, pp. 235-274.
[43] J.-C. Gui, L. Han, and W.-y. Cao, "Lamellar MXene: A novel 2D nanomaterial for electrochemical sensors," *Journal of Applied Electrochemistry,* vol. 51, pp. 1509-1522, 2021.
[44] N. Murugan, R. Jerome, M. Preethika, A. Sundaramurthy, and A. K. Sundramoorthy, "2D-titanium carbide (MXene) based selective electrochemical sensor for simultaneous detection of ascorbic acid, dopamine and uric acid," *Journal of Materials Science & Technology,* vol. 72, pp. 122-131, 2021.
[45] J. Rajendran, A. K. Sundramoorthy, D. Ganapathy, R. Atchudan, M. A. Habila, and D. Nallaswamy, "2D MXene/graphene nanocomposite preparation and its electrochemical performance towards the identification of nicotine level in human saliva," *Journal of Hazardous Materials,* vol. 440, p. 129705, 2022.

[46] S. Chen *et al.*, "Ti3C2T x MXene/nitrogen-doped reduced graphene oxide composite: a high-performance electrochemical sensing platform for adrenaline detection," *Nanotechnology*, vol. 32, no. 26, p. 265501, 2021.
[47] S. Mukherjee, A. Mukherjee, Z. Bytesnikova, A. M. Ashrafi, L. Richtera, and V. Adam, "2D graphene-based advanced nanoarchitectonics for electrochemical biosensors: Applications in cancer biomarker detection," *Biosensors and Bioelectronics*, p. 116050, 2024.
[48] W. Wang, H. Tang, L. Zhou, and Z. Li, "A Novel Label-Free Electrochemical Immunosensor for the Detection of Thyroid Transcription Factor 1 Using Ribbon-like Tungsten Disulfide-Reduced Graphene Oxide Nanohybrids and Gold Nanoparticles," *Molecules*, vol. 29, no. 2, p. 552, 2024.
[49] Z. Yan, Y. Bai, and L. Sun, "Adsorption of thiophene and SOx molecules on Cr-doped and Ti-doped graphene nanosheets: a DFT study," *Materials Research Express*, vol. 6, no. 12, p. 125067, 2019.
[50] Y. Li, Y. Chen, D. Deng, L. Luo, H. He, and Z. Wang, "Water-dispersible graphene/amphiphilic pyrene derivative nanocomposite: High AuNPs loading capacity for CEA electrochemical immunosensing," *Sensors and Actuators B: Chemical*, vol. 248, pp. 966-972, 2017.
[51] D. Zhang, J. Liu, C. Jiang, and P. Li, "High-performance sulfur dioxide sensing properties of layer-by-layer self-assembled titania-modified graphene hybrid nanocomposite," *Sensors and Actuators B: Chemical*, vol. 245, pp. 560-567, 2017.
[52] W. Li *et al.*, "UV light irradiation enhanced gas sensor selectivity of NO2 and SO2 using rGO functionalized with hollow SnO2 nanofibers," *Sensors and Actuators B: Chemical*, vol. 290, pp. 443-452, 2019.
[53] L. Qian, A. R. Thiruppathi, R. Elmahdy, J. van der Zalm, and A. Chen, "Graphene-oxide-based electrochemical sensors for the sensitive detection of pharmaceutical drug naproxen," *Sensors*, vol. 20, no. 5, p. 1252, 2020.
[54] X.-P. Chen *et al.*, "Sulfur dioxide and nitrogen dioxide gas sensor based on arsenene: a first-principle study," *IEEE Electron Device Letters*, vol. 38, no. 5, pp. 661-664, 2017.
[55] Y. Tang, Z. Liu, Z. Shen, W. Chen, D. Ma, and X. Dai, "Adsorption sensitivity of metal atom decorated bilayer graphene toward toxic gas molecules (CO, NO, SO2 and HCN)," *Sensors and Actuators B: Chemical*, vol. 238, pp. 182-195, 2017.
[56] H. Louis, K. Chukwuemeka, E. C. Agwamba, H. Y. Abdullah, and A. M. Pembere, "Molecular simulation of Cu, Ag, and Au-decorated Si-doped graphene quantum dots (Si@ QD) nanostructured as sensors for SO2 trapping," *Journal of Molecular Graphics and Modelling*, vol. 124, p. 108551, 2023.
[57] X. Wu *et al.*, "Graphene-based mesoporous frameworks with ultrahigh nitrogen contents for highly efficient and selective sulfur dioxide capture," *Chemical Engineering Journal*, vol. 412, p. 128677, 2021.
[58] S. Zhou, J. Liu, S. Pang, and Y. Gui, "Adsorption Characteristics of H2S and SO2 Gases on Cu2O Cluster-Modified Graphene Monolayer for Gas-Sensing Applications," *ACS omega*, vol. 8, no. 48, pp. 45763-45773, 2023.
[59] D. Chen, J. Tang, X. Zhang, H. Cui, and Y. Li, "Sulfur dioxide adsorbed on pristine and Au dimer decorated γ-graphyne: A density functional theory study," *Applied Surface Science*, vol. 458, pp. 781-789, 2018.
[60] J. Li, L. Pang, K. He, and L. Zhang, "Theoretical Study of The Gas Sensing Mechanism of N 3 &Ni Doped Double Vacancies Defect Graphene upon SF 6 Decompositions," *IEEE Access*, vol. 7, pp. 145567-145573, 2019.
[61] J. Wang *et al.*, "Is Mg17Al12 ductile or brittle? A theoretical insight," *Journal of Magnesium and Alloys*, vol. 11, no. 3, pp. 936-944, 2023.
[62] D. D. Roy, P. Roy, and D. De, "Electrically Doped Nano Devices: A First Principle Paradigm," *Advanced Nanoscale MOSFET Architectures: Current Trends and Future Perspectives*, pp. 125-141, 2024.
[63] M. G. Monfared and S. E. Hosseini, "New methods to increase PVR in gate controllable armchair graphene-boron nitride RTDs," *Optical and Quantum Electronics*, vol. 56, no. 4, p. 698, 2024.
[64] T. Tarun, P. Singh, H. Kaur, G. K. Walia, D. K. K. Randhawa, and B. Choudhary, "Defective GaAs nanoribbon–based biosensor for lung cancer biomarkers: a DFT study," *Journal of Molecular Modeling*, vol. 27, no. 9, p. 270, 2021.
[65] X. Gao, Q. Zhou, J. Wang, L. Xu, and W. Zeng, "Adsorption of SO2 molecule on Ni-doped and Pd-doped graphene based on first-principle study," *Applied Surface Science*, vol. 517, p. 146180, 2020.
[66] L. Shao *et al.*, "Sulfur dioxide molecule sensors based on zigzag graphene nanoribbons with and without Cr dopant," *Physics Letters A*, vol. 378, no. 7-8, pp. 667-671, 2014.
[67] C. Guo and T. Wang, "Zigzag direction nanoarchitectonics of monolayer GeSe for SO2 gas sensors with high sensitivity and selectivity: a first-principles study," *Applied Physics A*, vol. 128, no. 11, p. 975,

Journal Pre-proof

2022.

[68] R. Jyoti, M. Chauhan, B. Choudhary, and R. K. Sharma, "Density functional theory study of manganese doped armchair graphene nanoribbon for effective carbon dioxide gas sensing," *ES Energy & Environment*, vol. 18, pp. 47-55, 2022.

[69] M. Ali, S. Khan, F. Awwad, and N. Tit, "High gas-sensing selectivity of bilaterally edge-doped graphene nano-ribbons towards detecting NO2, O2 and SO3 gas molecules: Ab-initio investigation," *Applied Surface Science*, vol. 514, p. 145866, 2020.

Journal Pre-proof